Purdue University
Purdue e-Pubs

Other Nanotechnology Publications | Birck Nanotechnology Center

8-1-2008

Phonon runaway in carbon nanotube quantum dots

L Siddiqui
Purdue University, lsiddiqu@purdue.edu

A W. Ghosh
Department of Electrical and Computer Engineering, University of Virginia

Supriyo Datta
Birck Nanotechnology Center and Purdue University, datta@purdue.edu

Follow this and additional works at: http://docs.lib.purdue.edu/nanodocs

Siddiqui, L; Ghosh, A W.; and Datta, Supriyo, "Phonon runaway in carbon nanotube quantum dots" (2008). *Other Nanotechnology Publications.* Paper 93.
http://docs.lib.purdue.edu/nanodocs/93

This document has been made available through Purdue e-Pubs, a service of the Purdue University Libraries. Please contact epubs@purdue.edu for additional information.

Phonon runaway in carbon nanotube quantum dots

L. Siddiqui,[1] A. W. Ghosh,[2] and S. Datta[1]
[1]*NSF Network for Computational Nanotechnology, Purdue University, West Lafayette, Indiana 47907, USA*
[2]*Department of Electrical and Computer Engineering, University of Virginia, Charlottesville, Virginia 22903, USA*
(Received 17 September 2006; revised manuscript received 30 April 2007; published 24 August 2007)

We explore electronic transport in a nanotube quantum dot strongly coupled with vibrations and weakly with leads and the thermal environment. We show that the recent observation of anomalous conductance signatures in single-walled carbon nanotube quantum dots [B. J. LeRoy *et al.*, Nature (London) **395**, 371 (2004) and B. J. LeRoy *et al.*, Phys. Rev. B **72**, 075413 (2005)] can be understood quantitatively in terms of current driven "hot phonons" that are strongly correlated with electrons. Using rate equations in the many-body configuration space for the joint electron-phonon distribution, we argue that the variations are indicative of strong electron-phonon coupling requiring an analysis beyond the traditional uncorrelated phonon-assisted transport (Tien-Gordon) approach.

DOI: 10.1103/PhysRevB.76.085433 PACS number(s): 73.23.−b

I. INTRODUCTION

One of the significant challenges in microelectronics is controlling the rapidly increasing thermal budget associated with current flow through shrinking devices. Experimental[1–7] and theoretical[8–14] investigations are revealing intriguing aspects of the mutual effect of electronic and vibronic modes on each other. Nanoscale vibrations tend to couple strongly with electronic currents and weakly with their "macroenvironment," allowing them to be easily driven far from equilibrium. Understanding the dynamics of such electronically driven phonon runaway processes is crucial to the evolution of low-power devices, not to mention novel concepts like molecular motors and phonon lasers.[15]

In this paper, we develop a theoretical treatment of current driven nonequilibrium correlated phonon dynamics in nanoscale systems, and use this approach to analyze recent experiments on single-walled carbon nanotube (SWCNT) quantum dots (QDs).[1] Using a rate equation for correlated transport in the full many-body eigenspace of the coupled electron-phonon–lead-bath system, we explain novel spectroscopic features such as the anomalously large absorption sidebands arising from phonon runaway in suspended, Coulomb blockaded nanotubes (Fig. 1).

Our model also explains semiquantitative features of the experiment such as the amplitude variation of the Coulomb blockaded conductance peaks and their phonon sidebands, as a function of injected current. However, our model predicts a *linear* variation in phonon population with current, in contrast with experiments that show a *quadratic* variation.[1,2] We argue that a possible origin of this discrepancy is because our model explicitly incorporates the effect of strong electron-phonon correlation that is characteristic of these experiments, while the experimentally extracted variation was accomplished by employing a traditional Tien-Gordon analysis that implicitly treats the phonon contribution only through its mean-field oscillating potential acting on the electronic subsystem.[16]

Our paper thus serves a dual purpose: (i) it identifies transport signatures of the individual physical ingredients, such as the electronic energy levels and their Coulomb interaction that determine the main peak positions in Fig. 1, the phonon modes that determine the positions of their sidebands, and the couplings with the leads and the surrounding bath that determine the heights, respectively, of the main conductance peaks and their sidebands. (ii) Using general arguments as well as through the comparison between our theoretical model and experimental data, we establish the inadequacy of commonly employed "mean-field" treatments, such as the Tien-Gordon theory of phonon assisted tunneling,[16] in describing strongly correlated systems driven away from equilibrium. While our formalism involves standard techniques employing rate equations within the excitation spectrum of a many-body Hamiltonian, our emphasis lies in incorporating the various components, particularly the incoherence driven by the dynamics of the bath, and identifying specific signatures of the failure of mean-field theory in suspended nanotube dots characterized by strong nonequilibrium correlations.

II. MODEL

We use a model Hamiltonian H_D for a quantum dot with on-site energies ϵ_i, Coulomb interaction energy $U_{ii'}$, vibronic modes at energy $\hbar\omega_j$, and electron-phonon coupling λ_{ij} (Fig. 2). The total Hamiltonian including the contacts (H_C), the phonon bath (H_B), and their couplings with the dot (H_{DC}, H_{DB}) is

$$H = H_D + H_C + H_B + H_{DC} + H_{DB}, \tag{1}$$

$$H_D = H_{el} + H_{ph} + H_{el\text{-}ph}, \tag{2}$$

$$H_{el} = \sum_i \epsilon_i c_i^\dagger c_i + \frac{1}{2}\sum_{i,i',i\neq i'} U_{ii'} n_i n_{i'},$$

$$H_{ph} = \sum_j \hbar\omega_j a_j^\dagger a_j,$$

$$H_{el-ph} = \sum_{i,j} \lambda_{ij}\hbar\omega_j n_i (a_j^\dagger + a_j),$$

 ©2007 The American Physical Society

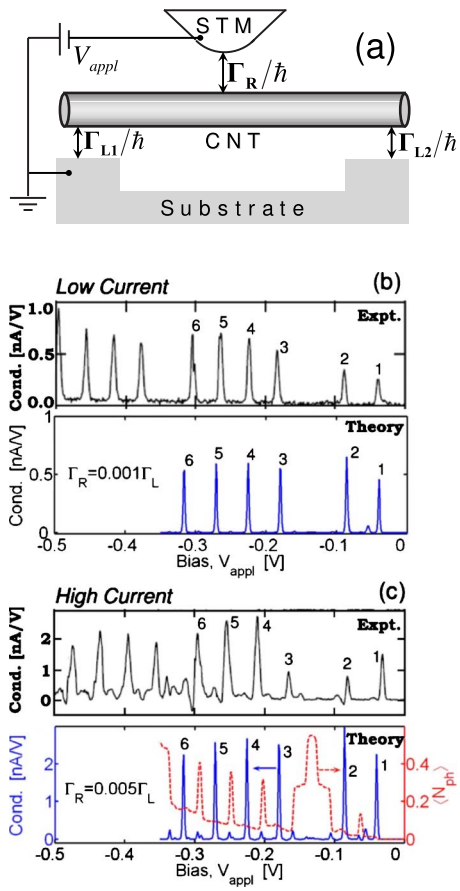

FIG. 1. (Color online) (a) Schematic of scanning tunnel microscope (STM) measurement on CNT QDs; (b) and (c) Experimental observation and theoretical calculation for CNT QDs at lower and higher current level [solid line: conductance; dashed line: $\langle N_{ph}\rangle$ in (c)]. $1,2,\ldots,6$ denotes the main Coulomb peaks. The parameters for the calculation are $\tilde{\epsilon}_1=\tilde{\epsilon}_2=24$ meV, $\tilde{\epsilon}_3=\tilde{\epsilon}_4=\tilde{\epsilon}_5=\tilde{\epsilon}_6=54$ meV, $\tilde{U}=27$ meV, $E_F=0$, $\hbar\omega_1=11.5$ meV, $\lambda_{11}=\lambda_{21}=\cdots=\lambda_{61}=1.6$, $\Gamma_{L1}+\Gamma_{L2}=7.5\times10^{-6}$ eV, $\beta=5\times10^{-8}$ eV, $\eta=0.6$, and $T=5$ K.

$$H_C=\sum_{k,\alpha\epsilon L,R}\epsilon_{k\alpha}d_{k\alpha}^{\dagger}d_{k\alpha}, \tag{3}$$

$$H_B=\sum_{l}\hbar\omega_l b_l^{\dagger}b_l, \tag{4}$$

$$H_{DC}=\sum_{i,k,\alpha}\tau_{ik\alpha}(d_{k\alpha}^{\dagger}c_i+d_{k\alpha}c_i^{\dagger}), \tag{5}$$

$$H_{DB}=\sum_{jl}\kappa_{jl}(b_l^{\dagger}+b_l)(a_j^{\dagger}+a_j), \tag{6}$$

where $c^{\dagger}$ (c) and $d^{\dagger}$ (d) are the electronic creation (destruction) operators for the dot and the leads, $n_i=c_i^{\dagger}c_i$ and $a^{\dagger}$ (a) and $b^{\dagger}$ (b) are the phonon creation (destruction) operators for the dot and the phonon bath, respectively. τ, ϵ_k, and κ represent, respectively, the dot-contact coupling, the contact band structure, and the coupling between the dot vibrations and the thermal bath.

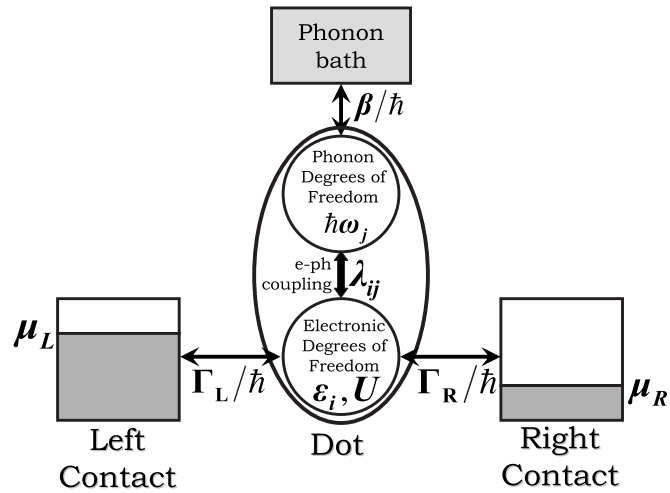

FIG. 2. The dot is electrically connected to the left (right) contact (with electron tunneling rates $\Gamma_{L,R}/\hbar$) and mechanically to the phonon bath (with a phonon escape rate of $\beta/\hbar$). The dot has electronic degrees of freedom ϵ_i and phonon degrees of freedom $\hbar\omega_j$ $(i,j=1,2,3,\ldots)$ with electron-phonon coupling λ_{ij}.

The electron-phonon coupling is eliminated using a standard unitary polaronic transformation $\tilde{H}=e^{S}He^{-S}$,[17] where $S=\Sigma_{i,j}\lambda_{ij}(a_j^{\dagger}-a_j)n_i$. This transformation renormalizes the on-site ($\tilde{\epsilon}_i$) and Coulomb ($\tilde{U}_{ii'}$) energies for the dot:

$$\tilde{H}_D=\sum_i\tilde{\epsilon}_i\tilde{c}_i^{\dagger}\tilde{c}_i+\frac{1}{2}\sum_{i,i'}\tilde{U}_{ii'}\tilde{n}_i\tilde{n}_{i'}+\sum_j\hbar\omega_j a_j^{\dagger}a_j, \tag{7}$$

$$\tilde{\epsilon}_i=\epsilon_i-\sum_j\lambda_{ij}^2\hbar\omega_j, \tag{8}$$

$$\tilde{U}_{ii'}=U_{ii'}-2\sum_j\lambda_{ij}\lambda_{i'j}, \tag{9}$$

where the "dressed" electron or polaronic annihilation operator

$$\tilde{c}_i=e^{S}c_ie^{-S}=cX \tag{10}$$

with $X=\exp\Sigma_j\lambda_{ij}(a_j-a_j^{\dagger})$ denoting the generator of the polaronic shift and

$$\tilde{a}_j=e^{S}a_je^{-S}=a_i-\sum_j\lambda_{ij}n_i \tag{11}$$

while preserving the electronic number operator $\tilde{n}_i=n_i$. At this point, we will simplify the model by considering only a single phonon mode, denoted by the index 1.

Current flow in this system involves single electron transitions between many-body states $|e_{Ne}^{i},k\rangle$ (k phonons and ith electronic level in the N_e electronic subspace) of the quantum dot, with matrix elements for the electronic destruction operator (for a derivation, see the Appendix, Sec. III):

$$\langle e^r_{Ne-1},p|\tilde{c}_i|e^s_{Ne},k\rangle = \begin{cases} e^{-\lambda_{i1}^2/2}(-\lambda_{i1})^{k-p}\sqrt{\frac{p!}{k!}}\mathcal{L}_p^{k-p}(\lambda_{i1}^2) & \text{for } k \geq p \\ e^{-\lambda_{i1}^2/2}(-\lambda_{i1})^{p-k}\sqrt{\frac{k!}{p!}}\mathcal{L}_k^{p-k}(\lambda_{i1}^2) & \text{for } p \geq k \end{cases}, \tag{12}$$

where $c_i|e^s_{Ne},k\rangle = |e^r_{Ne-1},k\rangle$ and $\mathcal{L}_p^q$ are the associated Laguerre polynomials. For total injection rates $\Gamma_\alpha/\hbar$ [$\alpha = L(\text{left})/R(\text{right})$] (Fig. 2), the transition rates are

$$\mathcal{R}^\alpha_{|e^r_{Ne-1},k\rangle\to|e^s_{Ne},p\rangle} = |\langle e^r_{Ne-1},p|\tilde{c}_i|e^s_{Ne},k\rangle|^2\frac{\Gamma_\alpha}{\hbar}f_\alpha(\mathcal{E}(|e^s_{Ne},p\rangle) - \mathcal{E}(|e^r_{Ne-1},k\rangle) - \eta|q|V_{appl}). \tag{13}$$

$f_{L,R}$ are the contact Fermi functions with electrochemical potentials $\mu_L = E_F$, $\mu_R = E_F - |q|V_{appl}$ at temperatures $T_{L,R}$, while the electrostatic voltage division factor η represents the fraction of the applied bias acting on the levels. Here $\mathcal{E}(|\rangle)$ stands for the total energy of the corresponding many-body eigenstate $|\rangle$ of the dot. Finally, the total injection rate Γ_α is given by Fermi's Golden Rule as $\Gamma_{i\alpha} = 2\pi\Sigma_k|\tau_{ik\alpha}|^2\delta(\epsilon_i - \epsilon_{k\alpha})$. We will use the wide-band approximation to assume $\Gamma_{i\alpha} = \Gamma_\alpha$.

It is worth emphasizing that the formalism for dealing with correlated transport is qualitatively different from its mean-field counterparts, which have traditionally been the popular way to describe quantum conduction.[18,19] For a strongly correlated dot, exclusion principle and charge quantization make it difficult to describe transport in terms of one-electron potentials, and each conducting level must instead be written as a difference between two many-body states. For instance, the electron affinity (the counterpart of a lowest unoccupied molecular orbital, or LUMO, level) is written as the difference in total energy between the neutral and anionic species. Electron transport at a given energy corresponds to a many-body transition corresponding to that transition energy, with partial probability given by the matrix elements described in Eq. (12).[20,21]

In our analysis, electrons enter or leave the dot by emitting or absorbing phonons, which in turn are coupled with their thermal environment, held at a bath temperature T_B, with an escape rate $\beta/\hbar$ (Fig. 2), that maintains a Boltzmann ratio between emission and absorption processes in the contact,

$$\mathcal{R}^{ph}_{|e^s_{Ne},k\rangle\to|e^s_{Ne},k+1\rangle} = \frac{\beta}{\hbar}(k+1)\exp\left(-\frac{\hbar\omega}{k_BT_B}\right),$$

$$\mathcal{R}^{ph}_{|e^s_{Ne},k\rangle\to|e^s_{Ne},k-1\rangle} = \frac{\beta}{\hbar}k. \tag{14}$$

The state transitions in the joint electron-phonon many-body space (with the loss of some correlation especially between degenerate levels) are described by a master equation describing the rate of populating and depopulating each many-body state:[20–23]

$$\frac{dP_{|e^s_{Ne},k\rangle}}{dt} = \sum_{r,N'_e,n}[P_{|e^r_{Ne'},n\rangle}\mathcal{R}_{|e^r_{Ne'},n\rangle\to|e^s_{Ne},k\rangle} - P_{|e^s_{Ne},k\rangle}\mathcal{R}_{|e^s_{Ne},k\rangle\to|e^r_{Ne'},n\rangle}] \tag{15}$$

together with the normalization condition for $P_{|e^s_{Ne},k\rangle}$, where $\mathcal{R} = \mathcal{R}^L + \mathcal{R}^R + \mathcal{R}^{ph}$.

Solving the rate equations at steady state gives us the current I and the steady state population of dot electrons $\langle N_{el}\rangle$ and phonons $\langle N_{ph}\rangle$:

$$I = q\sum_{N_e,N'_e,r,s,k,n}\text{sgn}(N'_e - N_e)P_{|e^s_{Ne},k\rangle}\mathcal{R}^L_{|e^r_{Ne'},n\rangle\to|e^s_{Ne},k\rangle},$$

$$\langle N_{el}\rangle = \sum_{s,N_e,k}N_eP_{|e^s_{Ne},k\rangle},$$

$$\langle N_{ph}\rangle = \sum_{s,N_e,k}kP_{|e^s_{Ne},k\rangle}, \tag{16}$$

where $\text{sgn}(x)$ is the signum function. This also gives us the phonon generation rate $\mathcal{G}^\alpha$ by the current and the phonon extraction rate $\mathcal{X}^{ph}$ (see the Appendix) by the bath:

$$\mathcal{G}^\alpha = \sum_{s,N_e,k}\sum_{r,N'_e,n}(n-k)P_{|e^s_{Ne},k\rangle}\mathcal{R}^\alpha_{|e^s_{Ne},k\rangle\to|e^r_{Ne'},n\rangle},$$

$$\mathcal{X}^{ph} = \sum_{s,N_e,k}\sum_{r,N'_e,n}(k-n)P_{|e^s_{Ne},k\rangle}\mathcal{R}^{ph}_{|e^s_{Ne},k\rangle\to|e^r_{Ne'},n\rangle} = \left(\frac{\beta}{\hbar}\right)\frac{\langle N_{ph}\rangle - N^{eq}_{ph}}{N^{eq}_{ph}+1}, \tag{17}$$

where N^{eq}_{ph} is the equilibrium phonon occupancy at the bath temperature.

The rate equations are schematically explained in Fig. 2. The inputs to these equations are the electron tunneling rates $\Gamma_{L,R}$, the phonon escape rate β, the electronic energy configuration ϵ_i, the phonon energy $\hbar\omega_j$, the charging energy U, and the electron-phonon coupling λ_{ij}. In our analysis we will set the lead and bath temperatures $T_{L,R}$ and T_B to be equal to the ambient temperature.

It is important to explain the need for a parametrized theory for correlated transport. The configuration space of a many-electron system scales exponentially with basis size, making it hard to include more predictive ingredients. The complexity of this system should, however, not be confused with frequently modeled longer molecules that have weak correlations. For those systems, one can greatly simplify the transport problem with averaged one-electron potentials[18,19] and build *ab initio* parameter-free theories. The problem here deals with a molecular dot with Hubbard interactions coupled with leads, phonons, and a thermal bath, and driven away from equilibrium by an applied voltage bias. While this complex interacting system is simply too complicated to model without a parametrized theory, the parameters we will employ are not widely adjustable, but are in fact constrained pretty rigidly by the experimental facts (details follow in

Sec.III A). Furthermore, our main conclusions are quite robust with respect to the choice of the parameters.

III. NONEQUILIBRIUM PHONON OCCUPATION IN CNT QD

A. Peaks in the conductance spectrum due to phonon-assisted tunneling

We will now apply our many-body rate equations to analyze recent experiments[1,2] on phonon-assisted tunneling in suspended SWCNT quantum dots. The experiment shows several striking features such as anomalously large phonon absorption peaks at low temperature (5 K) and a monotonic increase in phonon sideband amplitude with current [Figs. 1(b) and 1(c)]. Conductance peaks are observed in groups of 4, suggesting consecutive doubly spin-degenerate electronic levels in the Coulomb blockade regime. Sidebands are attributed to phonon-assisted tunneling through the radial breathing mode (RBM) of the SWCNT, known to predominate at low bias through its effect at the bottom of the conduction band.[24]

We will model the dot with a single phonon mode ($\hbar\omega_1$) corresponding to the RBM and six electronic energy levels—two lower energy degenerate levels ($\tilde{\epsilon}_1$ and $\tilde{\epsilon}_2$) and four higher energy degenerate ones ($\tilde{\epsilon}_3$, $\tilde{\epsilon}_4$, $\tilde{\epsilon}_5$, and $\tilde{\epsilon}_6$). The occurrence of the singly degenerate and the doubly degenerate discrete electronic levels in CNT QDs has been observed earlier.[25,26] We will assume that the tunneling rate $\Gamma_\alpha/\hbar$ and the phonon escape rate $\beta/\hbar$ are dispersionless, and use the same value for the couplings ($\lambda_{11}=\lambda_{21}=\cdots=\lambda_{61}$) of the RBM to all the electronic levels.[27]

In order to match experimental results, we find it necessary to consider electron addition levels only, and not electron removal levels lying below the equilibrium Fermi energy.[1,2] An analytical estimate of the height of the first two conductance peaks, corresponding to two degenerate levels at $\tilde{\epsilon}_{1,2}$, explains the justification behind this assumption. It can be shown that the height of the first two electron *removal* peaks should be proportional to $2\Gamma_L\Gamma_R/(2\Gamma_R+\Gamma_L)$ and $2\Gamma_L\Gamma_R/(\Gamma_R+\Gamma_L)-2\Gamma_L\Gamma_R/(2\Gamma_R+\Gamma_L)$,[20] assuming that the left contact injects electrons, the temperature is very low, and ignoring phonon sidebands—assumptions which are consistent with experimental conditions. However, this predicts, for $\Gamma_R \ll \Gamma_L$, that the height of the second peak should become zero, in contrast with the experiment [Fig. 1(b)]. The height of the first two electron *addition* peaks, under the same assumption, can be shown to be proportional to $2\Gamma_L\Gamma_R/(\Gamma_R+2\Gamma_L)$ and $2\Gamma_L\Gamma_R/(\Gamma_R+\Gamma_L)-2\Gamma_L\Gamma_R/(\Gamma_R+2\Gamma_L)$ which predicts, for $\Gamma_R \ll \Gamma_L$, that the peak heights should be equal, in agreement with experiment [Fig. 1(b)]. This suggests that the observed peaks arise from electron addition rather than removal.

Next, let us estimate the input parameters. The phonon energy $\hbar\omega_1$ was measured to be 11.5 meV (see Refs. 1 and 2) which, together with the separation between the main Coulomb peak and its first phonon emission sideband, yields a voltage-division factor $\eta \approx 0.6$. The polaron renormalized charging parameter $\tilde{U}$ is estimated to be 30 meV, as extracted from the separation between consecutive Coulomb peaks originating from the same degenerate set of levels. From the estimate of the phonon decay rate and the Q factor, β was determined to be $\sim 10^{-8}$ eV. In our calculations we varied the tunneling rates Γ_α and electron-phonon coupling constant λ_{i1} ($i=1,2,\ldots,6$) to match the experimental conductance levels.

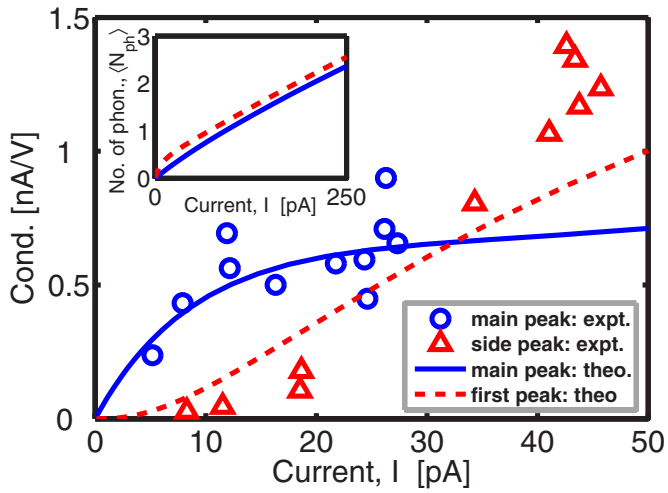

FIG. 3. (Color online) Variation of conductance with the current at the second Coulomb peak (at $V_{appl}=-0.1$ V) and its associated first phonon sidepeak (at $V_{appl}=-0.125$ V). Inset: Variation of the number of phonons with current at the above-mentioned conductance peaks. The parameters used to generate these results are $\tilde{\epsilon}_1=\tilde{\epsilon}_2=\tilde{\epsilon}=8$ meV, $\tilde{U}=12$ meV, $E_F=0$, $\hbar\omega_1=12.5$ meV, $\lambda_{11}=\lambda_{21}=2.1$, $\Gamma_L=5\times10^{-6}$ eV, $\Gamma_R=0.000\,05\Gamma_L$–$0.5\Gamma_L$, $\beta=5\times10^{-10}$ eV, $\eta=0.2$, and $T=5$ K.

Figures 1(b) and 1(c) show a comparison between the experiment and our calculations with the above parameters. Six levels seem sufficient to capture the essential physics, including the increase in the number of phonons between emission and absorption sidepeaks arising from the corresponding increase or decrease of phonon occupation at those bias points [Fig. 1(c)]. The calculated phonon number significantly exceeds the equilibrium value after each emission peak and drops considerably after absorption, indicating strongly correlated nonequilibrium phonon dynamics in this system. The weak phonon-substrate coupling β for suspended tubes leads to a phonon bottleneck whereby the current emits phonons faster than they are conducted away, leading to anomalous low-temperature absorption peaks that *even exceed* the corresponding emission peak heights on occasion. Such a phonon bottleneck can also create negative differnetial resistance due to self-heating [Ref. 30].

B. Variation of conductance with current

Experiment[1] shows a prominent quadratic dependence of the phonon occupancy on current. This variation is extracted indirectly from the observed variation in height of a main conduction peak and its associated first phonon sidepeak with current (Fig. 3), by applying a traditional Tien-Gordon model to fit it.[16] Note that these reported experimental results

are from a different CNT QD sample from the one corresponding to Figs. 1(b) and 1(c). So we will use a model with a different configuration of parameters to capture the essential characteristics of the experimental observations. In order to ascertain the conductance variation with current, we have replotted the reported normalized conductance, $(dI/dV_{appl})/(I/V_{appl})$ vs current, I to conductance $G = dI/dV_{appl}$ vs current I, using the known bias values V_{appl} (−0.1 V at main peak and −0.125 V at first sidepeak) and current values I at those peaks obtained from Ref. 1. The experimental observation shows that the main conductance peak initially increases with current and thereafter tends to saturate. On the other hand, the conductance at the first side peak gradually increases with current exponentially within the entire current range of the experiment.

To explore this variation we further simplify our model to just two degenerate single electronic levels at energy $\tilde{\epsilon}$. The simulation produces two Coulomb peaks and their associated phonon sidepeaks. To mimic the experimental procedure, we increased the current by varying the tunneling rate Γ_R of the STM tip. The calculated current dependences of the conductance at the second main peak (due to the direct tunneling at energy $\tilde{\epsilon}+\tilde{U}$) and its associated first phonon sidepeak at higher energy $(\tilde{\epsilon}+\tilde{U}+\hbar\omega_1)$ agree with the experimental trend (Fig. 3). However, we do not find $\langle N_{ph}\rangle$ varying as I^2 at the conduction peaks (Fig. 3, inset), but instead almost linearly within the experimental current range. The disagreement between our result and the claim made in Ref. 1 stems from the fundamental difference between our model and the Tien-Gordon model. Unlike our model, the Tien-Gordon model neglects the correlation between the electronic degrees of freedom and the phonon degrees of freedom by replacing the electron-phonon coupling Hamiltonian $H_{\text{el-ph}}$ with a mean-field oscillating potential $V=\langle \delta H_{\text{el-ph}}/\delta n\rangle$ which is proportional to the average position operator. For a particular phonon mode of frequency ω and in the absence of leads or baths, the position operator and thus the averaged phonon potential is simply proportional to $\cos \omega t$. Since the Bohr frequency of the electron in turn depends on this oscillating Hamiltonian, the resulting time-evolution operator and thus the electronic spectral functions end up with independent Fourier components whose spectral weights depend on Bessel functions, in other words, the Tien-Gordon expression. Crucial to the derivation of the Tien-Gordon model is the replacement of the electron-phonon coupling Hamiltonian by its mean-field time-dependent component ignoring leads and baths, which eliminates all correlation effects. This assumption is clearly inconsistent with our model that shows strongly correlated phonon dynamics, captured by the dimensionless electron-phonon coupling constant λ that is typically greater than unity, as mentioned in our figure captions. It is also noteworthy that the Tien-Gordon analysis requires coherent phonon dynamics. The phonons treated in our model are partly incoherent, because we ignore the off-diagonal terms in our electron-phonon density matrix to focus on occupation probabilities. In addition, the bath imposes thermodynamic averages on the diagonal correlators alone, acting as a physical source of incoherence in this system.

It is worth explaining why a single level does not suffice to capture this current variation. We find that the conductance of the main Coulomb peak, irrespective of the parameters chosen, varies linearly with current and does not saturate. Since the current prior to the main Coulomb peak is zero, the height of the main conductance peak $\sim I_{coul}/2k_BT$, where I_{coul} is the current plateau immediately past this voltage, the main broadening coming from temperature. This result, consistent with a test simulation with one single electron level (Fig. 4), also persists for the *first* in a series of Coulomb peaks in a multilevel system for the same reason. In all these examples, the main conductance peak can only vary linearly with the current, in contradiction with experiment, prompting us to look at higher peaks in a more complex, multileveled system. This requires us to adopt a more complex model with two single electron levels and to look at the variation at the second Coulomb peak and its associated phonon sidepeak. The results reported in the experiment [Figs. 4(a) and 4(b) of Ref. 1] were later confirmed to involve the variation of the second Coulomb peak and its associated phonon sidepeak.[29]

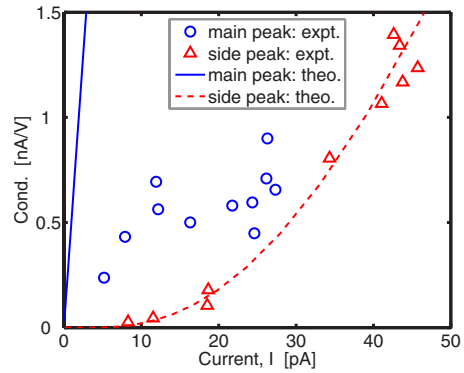

FIG. 4. (Color online) Simple one single electron level model does not match the experimental result at all. The values of the parameters used are $\tilde{\epsilon}_1=0.05$ eV, $\hbar\omega_1=12.5$ meV, $\lambda_{11}=1.7$, $\Gamma_L=1\times10^{-5}$ eV, $\Gamma_R=0.000\,05\Gamma_L$–$0.5\Gamma_L$, $\beta=5\times10^{-10}$ eV, $\eta=0.5$, and $T=5$ K.

We used our doubly degenerate single electron level model to explore the variation of the conductance for current values beyond the experimental current range, to project the characteristics under higher STM set current. The results are shown in Fig. 5. The conductance values at both the Coulomb peak and the first sidepeak show a nontrivial variation with current. The variation of the conductance at the Coulomb peak is compared to that (Fig. 5, inset) in the absence of electron-phonon coupling. We find that the coupling of electronic and phonon degrees of freedom significantly affects the Coulomb peak characteristics. In particular, while the trends match the experimental data up to the experimental current levels, we notice that at higher currents the main peak goes through a kink followed by a rise, while the sidepeak amplitude tends to saturate.

Finally, we look at the conductance variation with current for a quadruply degenerate single electron level model for a CNT QD that occasionally shows doubly spin degenerate shells. The conductance variation at each Coulomb peak and its associated first higher energy phonon sidepeak are shown in Fig. 6. The first Coulomb peak varies almost linearly with current (similar to Fig. 4), as we argued earlier. The conduc-

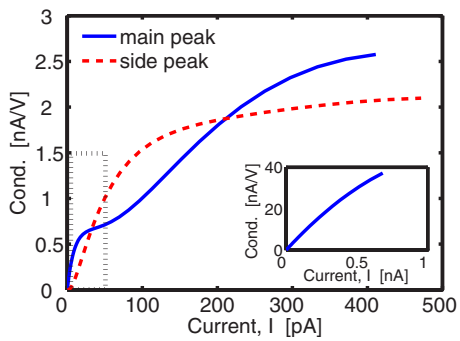

FIG. 5. (Color online) Variation of conductance with current for current values higher than the experimental range. Inset: The variation of conductance at the Coulomb peak in the absence of electron-phonon coupling. The values of the parameters used are the same as those of Fig. 3 (except that there is no coupling between electrons and phonons for the results in the inset). The region inside the dotted box is the range of experimental observation in Fig. 3.

tance variations at the other three peaks show the same qualitative trends as Fig. 5. From the qualitative similarity between Figs. 4–6, we see that the qualitative features of these variations are robust with respect to the values of the parameters that went into the model.

IV. CONCLUSION

We have studied strong electron-phonon coupled dynamics under nonequilibrium conditions using a many-electron rate equation approach, focusing on recent experiments on suspended nanotubes. From our calculations we argue that phonons in weakly coupled systems can be readily driven far from equilibrium, leading to anomalous signatures in the corresponding conductance spectrum and temperature dependences. Specifically, we expect the first Coulomb peak and its sideband to have a linear dependence on current, the higher Coulomb Blockade peak conductances should have a nontrivial variation with current with a kink at intermediate volatge, while the conductance of their corresponding vibronic sidebands should saturate (Fig. 6). Interesting extensions of this work would involve studying the imputations of nonequilibrium phonon dynamics for energy dissipation in nanoscale systems, and of maintaining phonon coherence by tuning their decay rates through their mechanical coupling with the substrate, and through phonon-phonon interactions controlled by the inherent nonlinearity of the lattice.

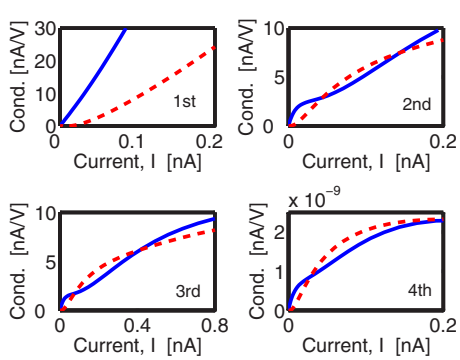

FIG. 6. (Color online) Variation of conductance with current for four degenerate single electron levels at the four Coulomb peaks (solid lines) and their associated first phonon sidepeaks (dashed lines). The values of the parameters used are $\tilde{\epsilon}_1=\tilde{\epsilon}_2=\tilde{\epsilon}_3=\tilde{\epsilon}_4=\tilde{\epsilon}=20$ meV, $\tilde{U}=30$ meV, $E_F=0$, $\hbar\omega_1=12.5$ meV, $\lambda_{11}=\lambda_{21}=\lambda_{31}=\lambda_{41}=2.1$, $\Gamma_L=5\times10^{-6}$ eV, $\Gamma_R=0.000\,05\Gamma_L$–$0.5\Gamma_L$, $\beta=5\times10^{-10}$ eV, $\eta=0.5$, and $T=5$ K.

ACKNOWLEDGMENTS

We would like to thank Cees Dekker and Brian LeRoy for sharing electronic data and for their valuable comments on an earlier version of this manuscript. We would also like to acknowledge NSF Network for Computational Technology (NCN) for providing the computational resources. This work was supported by DURINT and DARPA.

APPENDIX

In this section we show the derivation of some important analytical results. The derivations in Secs. I and II, which are already discussed in Refs. 12 and 17, have been worked out here to maintain continuity.

1. Derivation of Eqs. (10) and (11)

The terms like $e^S A e^{-S}$ are evaluated using

$$e^S A e^{-S} = A + [S,A] + (1/2\,!)[S,[S,A]] + \cdots . \quad \text{(A1)}$$

When $A=c_i$ we have

$$[S,c_i] = \sum_{h,j} \lambda_{hj}(a_j^\dagger - a_j)[c_h^\dagger c_h, c_i]$$

$$= \sum_{h,j} \lambda_{hj}(a_j^\dagger - a_j)[c_h^\dagger c_h c_i - c_i c_h^\dagger c_h]$$

$$= \sum_{h,j} \lambda_{hj}(a_j^\dagger - a_j)[-c_h^\dagger c_i c_h - c_i c_h^\dagger c_h]$$

$$= \sum_{h,j} \lambda_{hj}(a_j^\dagger - a_j)[(c_i c_h^\dagger - \delta_{i,h})c_h - c_i c_h^\dagger c_h]$$

$$= \sum_{h,j} \lambda_{hj}(a_j^\dagger - a_j)[-\delta_{i,h} c_h],$$

$$[S,c_i] = \sum_{i,j} \lambda_{ij}(a_j - a_j^\dagger)c_i, \quad \text{(A2)}$$

where δ is the kronecker delta function. Then,

$$[S,[S,c_i]] = \left[S, \sum_{i,j} \lambda_{ij}(a_j^\dagger - a_j)c_i\right]$$

$$= \sum_{i,j} [\lambda_{ij}(a_j^\dagger - a_j)] \sum_{h,j} [\lambda_{hj}(a_j^\dagger - a_j)][c_h^\dagger c_h, c_i],$$

$$[S,[S,c_i]] = \left[\sum_{i,j} \lambda_{ij}(a_j - a_j^\dagger)\right]^2 c_i, \tag{A3}$$

and so on. Putting all these results in Eq. (A1) we finally get Eq. (10). When $A=a_j$ we have

$$[S,a_j] = \sum_{i,h} n_i \lambda_{ih}[a_h^\dagger - a_h, a_j]$$

$$= \sum_{i,h} n_i \lambda_{ih}(a_h a_j - a_h^\dagger a_j - a_j a_h + a_j a_h^\dagger)$$

$$= \sum_{i,h} n_i \lambda_{ih} \delta_{j,h},$$

$$[S,a_j] = \sum_i n_i \lambda_{ij}. \tag{A4}$$

So afterwards, $[S,[S,a_j]]=[S,[S,[S,a_j]]]=\cdots=0$. Putting all these commutators in Eq. (A1) we get Eq. (11).

2. Derivation of Eqs. (7)–(9)

Applying the polaronic transformation,

$$\tilde{H}_D = \tilde{H}_{el} + \tilde{H}_{ph} + \tilde{H}_{el\text{-}ph}. \tag{A5}$$

Now the electronic portion

$$\tilde{H}_{el} = e^S H_{el} e^{-S},$$

$$\tilde{H}_{el} = \sum_i \epsilon_i \tilde{n}_i + \frac{1}{2}\sum_{i,i',i\neq i'} U_{ii'} \tilde{n}_i \tilde{n}_{i'}. \tag{A6}$$

The phonon portion

$$\tilde{H}_{ph} = e^S H_{ph} e^{-S},$$

$$\tilde{H}_{ph} = \sum_j \hbar\omega_j \tilde{a}_j^\dagger \tilde{a}_j$$

$$= \sum_j \hbar\omega_j \left(a_j^\dagger - \sum_i \lambda_{ij} n_i\right)\left(a_j - \sum_{i'} \lambda_{i'j} n_{i'}\right)$$

$$= \sum_j \hbar\omega_j a_j^\dagger a_j + \sum_{i,i',j} \hbar\omega_j \lambda_{ij}\lambda_{i'j} n_i n_{i'}$$

$$- \sum_{i,j} \hbar\omega_j \lambda_{ij} n_i a_j - \sum_{i',j} \hbar\omega_j \lambda_{i'j} n_{i'} a_j^\dagger,$$

$$\tilde{H}_{ph} = \sum_j \hbar\omega_j a_j^\dagger a_j + \sum_{i,i',j,i\neq i'} \hbar\omega_j \lambda_{ij}\lambda_{i'j} \tilde{n}_i \tilde{n}_{i'}$$

$$+ \sum_{i,j} \lambda_{ij}^2 \hbar\omega_j \tilde{n}_i - \sum_{i,j} \hbar\omega_j \lambda_{ij} \tilde{n}_i (a_j^\dagger + a_j), \tag{A7}$$

where we have used $n_i n_i = n_i = \tilde{n}_i$. Now, finally, the electron-phonon coupling term

$$\tilde{H}_{el-ph} = e^S H_{el-ph} e^{-S},$$

$$\tilde{H}_{el-ph} = \sum_{i,j} \lambda_{ij} \hbar\omega_j \tilde{n}_i (\tilde{a}_j^\dagger + \tilde{a}_j)$$

$$= \sum_{i,j} \hbar\omega_j \lambda_{ij} \tilde{n}_i \left(a_j^\dagger + a_j - \sum_{i'} \lambda_{i'j} n_{i'}^\dagger - \sum_{i'} \lambda_{i'j} n_{i'}\right)$$

$$= \sum_{i,j} \hbar\omega_j \lambda_{ij} \tilde{n}_i (a_j^\dagger + a_j) - 2\sum_{i,i',j} \hbar\omega_j \lambda_{ij}\lambda_{i'j} \tilde{n}_i \tilde{n}_{i'},$$

$$\tilde{H}_{el-ph} = \sum_{i,j} \hbar\omega_j \lambda_{ij} \tilde{n}_i (a_j^\dagger + a_j) - 2\sum_{i,j} \lambda_{ij}^2 \hbar\omega_j \tilde{n}_i$$

$$- 2\sum_{i,i',j,i\neq i'} \hbar\omega_j \lambda_{ij}\lambda_{i'j} \tilde{n}_i \tilde{n}_{i'}. \tag{A8}$$

Substituting Eqs. (A6)–(A8) in Eq. (A5) we get the results of Eqs. (7)–(9).

3. Derivation of Eq. (12)

We will start from

$$\langle e_{Ne-1}^r, p|\tilde{c}_i|e_{Ne}^s, k\rangle = \langle e_{Ne-1}^r, p|c_i X|e_{Ne}^s, k\rangle.$$

Now since $c_i|e_{Ne}^s, p\rangle = |e_{Ne-1}^r, p\rangle$ it follows that

$$\langle e_{Ne-1}^r, p|\tilde{c}_i|e_{Ne}^s, k\rangle = \langle e_{Ne}^s, p|X|e_{Ne}^s, k\rangle.$$

For one phonon mode $X=\exp[\lambda_{i1}(a_1 - a_1^\dagger)]$. Then

$$\langle e_{Ne-1}^r, p|\tilde{c}_i|e_{Ne}^s, k\rangle = \langle e_{Ne}^s, p|e^{\lambda_{i1}(a_1 - a_1^\dagger)}|e_{Ne}^s, k\rangle.$$

Using $e^{\lambda_{i1}(a_1 - a_1^\dagger)} = e^{-\lambda_{i1} a_1^\dagger} e^{\lambda_{i1} a_1} e^{-\lambda_{i1}^2/2}$:

$$\langle e_{Ne-1}^r, p|\tilde{c}_i|e_{Ne}^s, k\rangle = e^{-\lambda_{i1}^2/2} \langle e_{Ne}^s, p|e^{-\lambda_{i1} a_1^\dagger} e^{\lambda_{i1} a_1}|e_{Ne}^s, k\rangle. \tag{A9}$$

By simple algebra,

$$e^{\lambda_{i1} a_1}|e_{Ne}^s, k\rangle = \sum_{l=0}^{\infty} \frac{(\lambda_{i1})^l}{l!}(a_1)^l |e_{Ne}^s, k\rangle,$$

$$e^{\lambda_{i1} a_1}|e_{Ne}^s, k\rangle = \sum_{l=0}^{k} \frac{(\lambda_{i1})^l}{l!}\left[\frac{k!}{(k-l)!}\right]^{1/2} |e_{Ne}^s, k-l\rangle, \tag{A10}$$

and similarly

$$\langle e_{Ne}^s, p|e^{-\lambda_{i1} a_1^\dagger} = \sum_{m=0}^{p} \langle e_{Ne}^s, p-m|\frac{(-\lambda_{i1})^m}{m!}\left[\frac{p!}{(p-m)!}\right]^{1/2}. \tag{A11}$$

From Eqs. (A9)–(A11),

$$\langle e^r_{Ne-1},p|\tilde{c}_i|e^s_{Ne},k\rangle = e^{-\lambda_{i1}^2/2}\sum_{m=0}^{p}\sum_{l=0}^{k}\left[\frac{(\lambda_{i1})^l(-\lambda_{i1})^m}{m\,!\,l!}\times\frac{(p\,!\,k\,!\,)^{1/2}}{\{(p-m)\,!\,(k-l)\,!\,\}^{1/2}}\delta_{p-m,k-l}\right]. \tag{A12}$$

For the case of $k \geq p$, to remove the Kronecker delta function, we substitute $l=k-p+m$ in Eq. (A12):

$$\begin{aligned}\langle e^r_{Ne-1},p|\tilde{c}_i|e^s_{Ne},k\rangle &= e^{-\lambda_{i1}^2/2}\sum_{m=0}^{p}\left[\frac{(\lambda_{i1})^{k-p+m}(-\lambda_{i1})^m}{m\,!\,(k-p+m)!}\times\frac{(p\,!\,k\,!\,)^{1/2}}{(p-m)!}\right]\\ &= e^{-\lambda_{i1}^2/2}\sum_{m=0}^{p}\frac{(-1)^m(\lambda_{i1})^{k-p}(\lambda_{i1}^2)^m(k\,!\,p\,!\,)^{1/2}}{m\,!\,(k-p+m)\,!\,(p-m)!}\\ &= e^{-\lambda_{i1}^2/2}(\lambda_{i1})^{k-p}\sqrt{\frac{p!}{k!}}\times\sum_{m=0}^{p}\frac{(-1)^m\{(k-p)+p\}\,!\,(\lambda_{i1}^2)^m}{m\,!\,\{(k-p)+m\}\,!\,(p-m)!}.\end{aligned}$$

The summed series is nothing but associated Laguerre polynomial $\mathcal{L}_p^{k-p}(\lambda_{i1}^2)$. So finally, we get

$$\langle e^r_{Ne-1},p|\tilde{c}_i|e^s_{Ne},k\rangle = e^{-\lambda_{i1}^2/2}(\lambda_{i1})^{k-p}\sqrt{\frac{p!}{k!}}\mathcal{L}_p^{k-p}(\lambda_{i1}^2) \quad \text{for } k \geq p.$$

Following the exact same procedure, we can show that

$$\langle e^r_{Ne-1},p|\tilde{c}_i|e^s_{Ne},k\rangle = e^{-\lambda_{i1}^2/2}(\lambda_{i1})^{p-k}\sqrt{\frac{k!}{p!}}\mathcal{L}_k^{p-k}(\lambda_{i1}^2) \text{ for } p \geq k.$$

4. Derivation of Eq. (17)

From Eqs. (14), we can see that the phonon bath induces a transition between only those two states which have the exact same electronic configuration and phonon number differing by 1. So we can write

$$\begin{aligned}\mathcal{X}^{ph} &= \sum_{s,Ne,k}\sum_{r,Ne',n}(k-n)P_{|e^s_{Ne},k\rangle}\mathcal{R}^{ph}_{|e^s_{Ne},k\rangle\to|e^r_{Ne'},n\rangle}\\ &= \sum_{s,N_e,k}(k-k\mp 1)P_{|e^s_{Ne},k\rangle}\mathcal{R}^{ph}_{|e^s_{Ne},k\rangle\to|e^s_{Ne},k\pm 1\rangle}\\ &= \sum_{s,N_e}\sum_{k=1}^{\infty}P_{|e^s_{Ne},k\rangle}\mathcal{R}^{ph}_{|e^s_{Ne},k\rangle\to|e^s_{Ne},k-1\rangle}\\ &\quad -\sum_{s,N_e}\sum_{k=0}^{\infty}P_{|e^s_{Ne},k\rangle}\mathcal{R}^{ph}_{|e^s_{Ne},k\rangle\to|e^s_{Ne},k+1\rangle}\\ &= \frac{\beta}{\hbar}\sum_{s,N_e}\sum_{k=0}^{\infty}P_{|e^s_{Ne},k\rangle}\left[k-(k+1)\exp\left(-\frac{\hbar\omega}{k_BT_B}\right)\right]\\ &= \left(\frac{\beta}{\hbar}\right)\left[1-\exp\left(-\frac{\hbar\omega}{k_BT_B}\right)\right]\sum_{s,N_e}\sum_{k=0}^{\infty}kP_{|e^s_{Ne},k\rangle}-\left(\frac{\beta}{\hbar}\right)\\ &\quad\times\exp\left(-\frac{\hbar\omega}{k_BT_B}\right)\sum_{s,N_e}\sum_{k=0}^{\infty}P_{|e^s_{Ne},k\rangle}.\end{aligned}$$

So, from Eq. (16) and the normalization condition

$$\begin{aligned}\mathcal{X}^{ph} &= \left(\frac{\beta}{\hbar}\right)\left\{\langle N_{ph}\rangle\left[1-\exp\left(-\frac{\hbar\omega}{k_BT_B}\right)\right]-\exp\left(-\frac{\hbar\omega}{k_BT_B}\right)\right\}\\ &= \left(\frac{\beta}{\hbar}\right)\left[\langle N_{ph}\rangle\left(1-\frac{N_{ph}^{eq}}{N_{ph}^{eq}+1}\right)-\frac{N_{ph}^{eq}}{N_{ph}^{eq}+1}\right],\end{aligned}$$

$$\mathcal{X}^{ph} = \left(\frac{\beta}{\hbar}\right)\frac{\langle N_{ph}\rangle - N_{ph}^{eq}}{N_{ph}^{eq}+1},$$

where $N_{ph}^{eq}=\{\exp[\hbar\omega/(k_BT)]-1\}^{-1}$.

[1] B. J. LeRoy, S. G. Lemay, J. Kong, and C. Dekker, Nature (London) **395**, 371 (2004).
[2] B. J. LeRoy, J. Kong, V. K. Pahilwani, C. Dekker, and S. G. Lemay, Phys. Rev. B **72**, 075413 (2005).
[3] H. Park, J. Park, A. K. L. Lim, E. H. Anderson, A. P. Alivisatos, and P. L. McEuen, Nature (London) **407**, 57 (2000).
[4] W. Wang, T. Lee, I. Kretzschmar, and M. Reed, Nano Lett. **4**, 643 (2004).
[5] L. H. Yu, Z. K. Keane, J. W. Ciszek, L. Cheng, M. P. Stewart, J. M. Tour, and D. Natelson, Phys. Rev. Lett. **93**, 266802 (2004).
[6] A. N. Pasupathy, J. Park, C. Chang, A. V. Soldatov, S. Lebedkin, R. C. Bialczak, J. E. Grose, L. A. K. Donev, J. P. Sethna, D. C. Ralph, and P. L. McEuen, Nano Lett. **5**, 203 (2005).
[7] E. Pop, D. Mann, J. Cao, Q. Wang, K. Goodson, and H. Dai, Phys. Rev. Lett. **95**, 155505 (2005).
[8] D. Boese and H. Schoeller, Europhys. Lett. **54**, 668 (2001).
[9] K. D. McCarthy, N. Prokof'ev, and M. T. Tuominen, arXiv:cond-mat/0205419.
[10] S. Braig and K. Flensberg, Phys. Rev. B **68**, 205324 (2003).
[11] A. Mitra, I. Aleiner, and A. J. Millis, Phys. Rev. B **69**, 245302 (2003).
[12] A. S. Alexandrov and A. M. Bratkovsky, Phys. Rev. B **67**, 235312 (2003); arXiv:cond-mat/0606366.
[13] V. Aji, J. E. Moore, and C. M. Varma, Int. J. Nanosci. **3**, 255 (2004).
[14] J. Koch, M. Semmelhack, F. von Oppen, and A. Nitzan, Phys. Rev. B **73**, 155306 (2006).
[15] T. Seideman, J. Phys.: Condens. Matter **15**, R521 (2003).
[16] P. K. Tien and J. P. Gordon, Phys. Rev. **129**, 647 (1963).
[17] G. D. Mahan, *Many Particle Physics (Physics of Solids and Liq-*

uids), 3rd Ed. (Plenum, New York, 2000).
[18] P. S. Damle *et al.*, Chem. Phys. **281**, 171 (2002).
[19] M. Di Ventra, S. T. Pantelides, and N. D. Lang, Phys. Rev. Lett. **84**, 979 (2000); J. Taylor, H. Guo, and J. Wang, Phys. Rev. B **63**, 245407 (2001); E. G. Emberly and G. Kirczenow, *ibid.* **58**, 10911 (1998); P. A. Derosa and J. M. Seminario, J. Phys. Chem. B **105**, 471 (2001); Y. Q. Xue and M. A. Ratner, Int. J. Quantum Chem. **102**, 911 (2005); J. J. Palacios *et al.*, Nanotechnology **13**, 1 (2002); M. Brandbyge, J. L. Mozos, P. Ordejon, J. Taylor, and K. Stokbro, Phys. Rev. B **65**, 165401 (2002).
[20] B. Muralidharan, A. W. Ghosh, and S. Datta, Phys. Rev. B **73**, 155410 (2006).
[21] S. Datta, *Quantum Transport: Atom to Transistor*, 2nd Rev. Ed. (Cambridge University Press, Cambridge, England, 2005).
[22] C. W. J. Beenakker, Phys. Rev. B **44**, 1646 (1991).
[23] F. Elste and C. Timm, Phys. Rev. B **71**, 155403 (2005).
[24] V. Perebeinos, J. Tersoff, and P. Avouris, Phys. Rev. Lett. **94**, 086802 (2005).
[25] W. Liang, M. Bockrath, and H. Park, Phys. Rev. Lett. **88**, 126801 (2002).
[26] D. H. Cobden and J. Nygard, Phys. Rev. Lett. **89**, 046803 (2002).
[27] Note that assumptions of uniform electron-phonon coupling and charging energy can be easily relaxed, as demonstrated in Ref. 28.
[28] Katja C. Nowack and Maarteen R. Wegewijs, arXiv:cond-mat/0506552.
[29] C. Dekker *et al.* (private communications).
[30] E. Pop, D. Mann, J. Cao, Q. Wang, K. Goodson, and H. Dailý, Phys. Rev. Lett. **95**, 155505 (2005).